Calcium-dependent regulation of auxin transport in plant development

Wei, X.

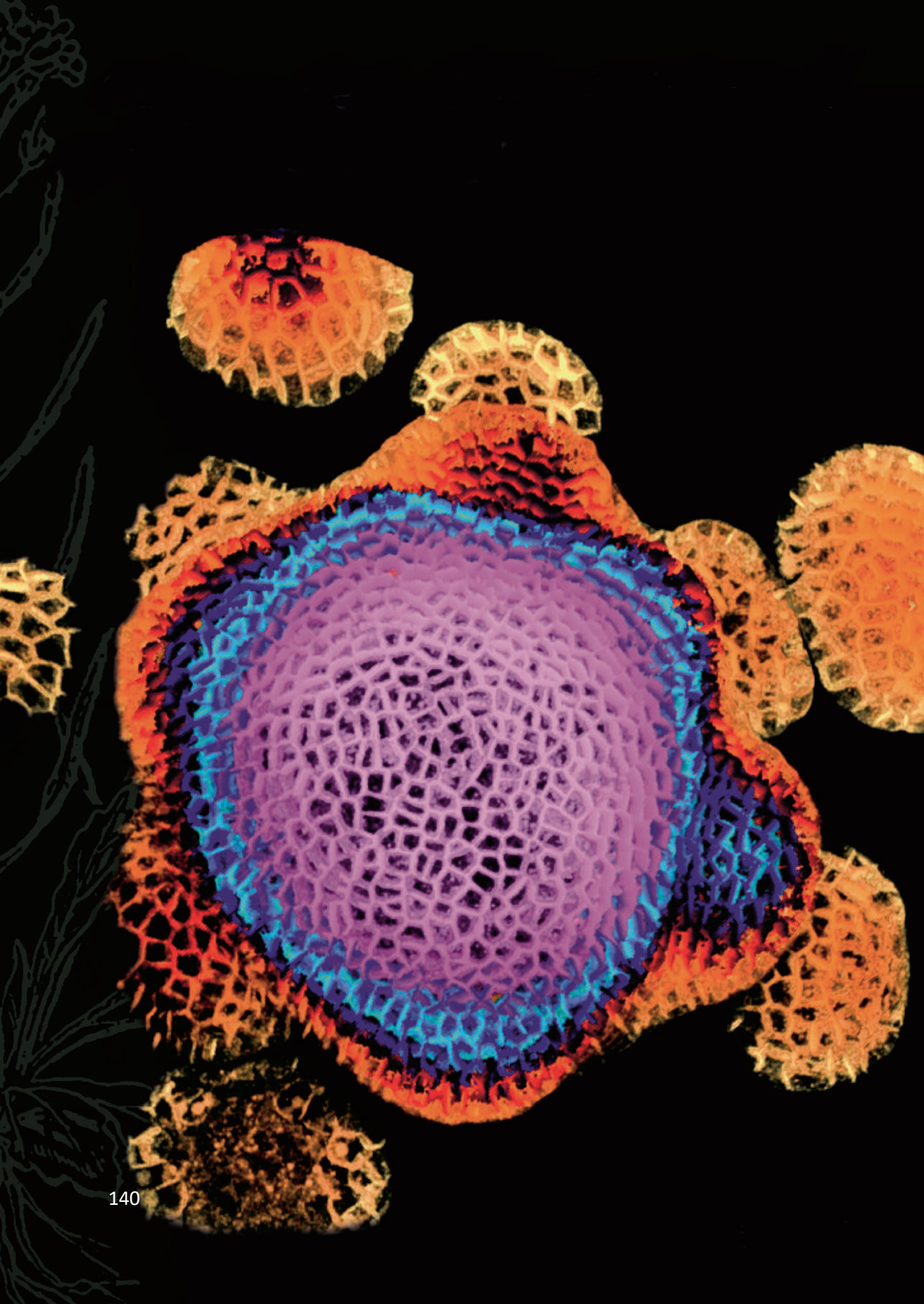

Chapter 4

Calcium-regulated PINOID kinase activity is required for a robust spiral phyllotaxis in the Arabidopsis inflorescence

Xiaoyu Wei[1] and Remko Offringa[1]*

[1]Plant Developmental Genetics, Institute of Biology Leiden, Leiden University, Sylviusweg 72, 2333 BE, Leiden, Netherlands

*Author for correspondence: r.offringa@biology.leidenuniv.nl

The results in this Chapter are included in the following publication: **Wei, X.Y.,** Fan, Y.W.,.….Offringa, R*. Calcium-regulated PINOID kinase activity is required for a robust spiral phyllotaxis in the Arabidopsis inflorescence (In preparation).

Abstract

Plant leaves and flowers are generated by the shoot apical meristem (SAM) following a precise spatio-temporal pattern, leading to a regular organ arrangement on a plant stem, also known as phyllotaxis. The plant hormone auxin plays a central role in establishing this pattern, as PIN-FORMED1 (PIN1) carrier-generated auxin maxima in the L1 layer of the SAM are the sites of organ initiation. The PINOID (PID) kinase is an important factor in this process, as it activates PIN proteins and directs their polarity to form convergence points where auxin maxima and organs are initiated. In the previous two Chapters of this thesis, we showed that PID interacts in a Ca^{2+}-dependent manner with CALMODULIN-LIKE 12/TOUCH 3 (CML12/TCH3) and 10 closely related calmodulins (CaMs) and CMLs. To study the role of PID-CaM/CML binding in plant development, we expressed 'untouchable' PID versions, specifically disrupted in their CaM/CML binding domain, in the *pid* loss-of-function mutant background. Initial phenotypic analysis of these plants suggested that the mutant PID versions were fully functional, as they complemented the pin-like inflorescence phenotype of the *pid* mutant. However, closer inspection of the inflorescences of these plants showed clear defects in the spiral phyllotaxis, ranging from deviating divergence angles between subsequent flowers and fruits to the simultaneous initiation of flower primordia. These phenotypes were reflected in the increased number and randomized position of PIN convergence points and auxin maxima in the inflorescence meristems of the 'untouchable' PID expressing plants. Together our data indicate that Ca^{2+}-dependent regulation of PID activity by CaM/CML binding is required for the accurate spatio-temporal positioning in the SAM of one auxin maximum at a time. We hypothesise that the PID – CAM/CML interaction integrates hormonal and abiotic signals that trigger elevations in $[Ca^{2+}]_{cyt}$, such as auxin and mechanical stress, to generate robustness in the spiral phyllotaxis that is typical for the Arabidopsis inflorescence.

Keywords: *Arabidopsis thaliana*, polar auxin transport, calcium signalling, mechanical stress, PINOID (PID) kinase, Calmodulin (CaM), Calmodulin-like (CML), phyllotaxis, inflorescence meristem (IM)

Introduction

Phyllotaxis is the regular arrangement of aerial organs, such as leaves and flowers, around the stem of a plant. These organs are generated from the shoot apical meristems (SAMs) of the plant, which includes the vegetative shoot apical meristem (SAM) generating leaves and the SAM-derived inflorescence meristem (IM) and floral meristem (FM) respectively generating flowers and floral organs. These SAMs comprise four functional zones: the central zone (CZ), peripheral zone (PZ), organizing center (OC), and rib zone (RZ) (Lyndon, 1998; Xue et al., 2020). Lateral organ primordia are initiated from the PZ and this process is triggered by local accumulation of the plant hormone auxin (Kuhlemeier and Reinhardt, 2001). Thus, phyllotaxis is determined by the dynamic and patterned auxin distribution at SAMs (Reinhardt et al., 2000; Reinhardt et al., 2003).

Auxin accumulation and distribution are for an important part mediated by polar auxin transport (PAT), which depends on the “long” PIN-FORMED (PIN) auxin efflux carriers, as their polar subcellular localization determines the directionality of PAT (Petrasek et al., 2006; Wisniewska et al., 2006; Zwiewka et a., 2019). It has been reported that the distribution of auxin in the L1 layer of SAMs through PIN1 is pivotal to the establishment of stable phyllotactic patterns (Jönsson et al., 2006; Smith et al., 2006; Stoma et al., 2008; Bhatia and Heisler, 2018). In the *Arabidopsis thaliana* (Arabidopsis) *pin-formed1* (*pin1*) mutant, aberrant inflorescences develop, characterized by the absence of flowers and a naked "pin-like" stem (Okada et al., 1991). PIN1 is strongly expressed in the SAMs, where it is

mainly found in the L1 layer, especially at the sites of incipient primordia formation (Reinhardt et al., 2003; Benková et al., 2003; Heisler et al., 2005). PIN1 polarizes towards the initiation site, forming a convergence pattern to generate an auxin maximum that triggers organ initiation. Together with the *pin1* mutant phenotype, this supports a direct role for PIN1 polarity in phyllotactic patterning (Reinhardt et al., 2003; Benková et al., 2003; Heisler et al., 2005; Bhatia et al., 2016). The polarization of PIN1 is regulated by the protein kinase PINOID (PID), a well-characterized regulator of PIN1 polarity. PID belongs to the AGC3 clade of the plant-specific family of AGCVIII protein kinases (Rademacher and Offringa, 2012). Together with its homologs WAG1 and WAG2, PID can induce a rootward(basal)-to-shootward(apical) shift in PIN polarity by phosphorylating serine residues in three conserved TPRXS motifs within the large central hydrophilic loop (PIN-HL) of "long" PIN proteins (Friml et al., 2004; Michniewicz et al., 2007; Huang et al., 2010; Dhonukshe et al., 2010). Interestingly, MITOGEN-ACTIVATED PROTEIN KINASES (MPK) 4 and 6 have been reported to phosphorylate the threonines in the same three TPRXS motifs of PIN1, leading to reduced plasma membrane (PM) abundance of PIN1 (Dory et al., 2018). Next to the three AGC3 clade kinases, members from the AGC1 clade of ACGVIII protein kinases, such as D6PK and PAX, have been shown to phosphorylate PIN proteins at different but also overlapping serine residues. Unlike the AGC3 kinases, phosphorylation by the AGC1 kinases does not cause a shift in polarity, but like AGC3 kinase-mediated phosphorylation it was reported to trigger PIN auxin efflux activity (Zourelidou et al., 2014; Barbosa et al., 2018; Marhava et al., 2018).

In addition to these kinases, various external stimuli (Heisler et al., 2010; Goh et al., 2012; Zhang et al., 2011; Li et al., 2019) and endogenous cues (Friml et al., 2003; Benková et al., 2003; Kleine-Vehn et al., 2011) have been reported to influence PIN polarity. The mechanism behind these influences is still largely unclear. External and endogenous cues cause signal-specific and tissue-specific changes in the concentration of cytosolic Ca^{2+} ($[Ca^{2+}]_{cyt}$), which are deciphered through the

action of Ca^{2+} sensors (Roberts and Harmon, 1992; Vogel, 1994). These sensors can be classified into two major groups: sensor relays, including Calmodulin/CaM-like proteins (CaM/CMLs) and Calcineurin B-like proteins (CBLs), and sensor responders, such as calcium-dependent protein kinases (CPKs) (Sanders et al., 2002).

Surprisingly, studies reporting molecular evidence for the involvement of Ca^{2+} signalling in the modulation of PAT are still limited. Recently, CPK29 was found to directly interpret Ca^{2+} signals from internal and external triggers, modulating PIN trafficking and polarity by phosphorylating another serine than the AGC or MAPK kinases in the PIN1-HL (Lee et al., 2021). In tomato, StCDPK1 has been reported to phosphorylate *StPIN4 in vitro*, suggesting a possible role in regulating StPIN4 polarity (Santin et al., 2017). Moreover, the CDPK related kinase CRK5 translates Ca^{2+} oscillations into altered PIN2 polarity by direct phosphorylation of the PIN2-HL (Rigó et al., 2013). Previously, we identified CALMODULIN-LIKE 12/TOUCH 3/ (CML12/TCH3) and the small EF-Hand protein, PID-BINDING PROTEIN 1 (PBP1) as interacting partners of PID (Benjamins et al., 2003). These findings provided one of the first molecular clues how Ca^{2+} signalling might modulate auxin transport polarity. Later, the inositol triphosphate (IP_3)-dependent $[Ca^{2+}]_{cyt}$ was implied in apical-basal PIN polarity and the activity of the AGC3 kinases (Zhang et al., 2011), which strengthened our model that the AGC3 kinases link Ca^{2+} signalling to PIN polarity.

In Chapter 2 of this thesis, we focussed on the PID-CML12/TCH3 interaction, showing that PID interacts with all seven Arabidopsis Calmodulins (CaMs) and with the four most closely related CMLs, CML8, CML10, CML11 and CML12/TCH3. Mutant and expression analyses indicated that there is considerable functional redundancy among the genes encoding the PID-interacting CaM/CMLs. This, together with the promiscuous interaction of CaM/CMLs with many different proteins, makes it very unlikely that (multiple) *cam/cml* loss-of-function mutants will specifically reveal the role of the PID-CaM/CML interaction in plant

development. Considering the observation that the PID-CaM/CML interaction leads to sequestration of PID from the PM, we fine mapped the CaM/CML interaction domain in PID to an amphipathic alpha helix in the insertion domain (ID) in the catalytic core of the kinase. Substitution of several of the positively charged arginines in the helix by alanines resulted in functional but 'untouchable' PID kinase versions (Chapter 3).

Here we used lines expressing the 'untouchable' PID version from the *PID* promoter in the *pid* loss-of-function mutant background to reveal the role of Ca^{2+}-regulation of PID activity in plant development. Our results show that disruption of the Ca^{2+}-dependent PID-CaM/CML interaction leads to significant defects in the spiral phyllotaxis generated by the Arabidopsis IM. Typically, more flower primordia were initiated at the same time, correlating with the simultaneous occurrence of multiple PIN1-generated auxin maxima. Based on these results we propose a model where the Ca^{2+}-dependent PID-CaM/CML interaction, possibly induced by local mechanical stress in the IM, is required to limit organ initiation by PIN1-mediated generation of a single auxin maximum at a time, thereby maintaining the regular spiral phyllotaxis.

Results

'Untouchable' PID does not alter seedling development or flowering time

In Chapter 3 we showed that disruption of the amphipathic alpha helix in the PID ID by substitution of arginines by alanines gave rise to PID versions (PID(R2A), PID(R3A) and PID(R5A)) that failed to interact with the CaM/CMLs ('untouchable'), but were functional based on the overexpression phenotypes and a rescue of the pin-like inflorescence phenotype of the *pid-14* loss-of-function mutant, when expressed as PID-YFP fusion under the *PID* promoter. At least 43 transgenic lines were obtained for each construct (*pPID:PID-YFP* and three

pPID:PID(R→A)-YFP constructs), and at least two single locus homozygous lines in *pid-14* homozygous background were used for further analysis.

A systematic phenotypic study showed no obvious differences between the *pPID:PID(R→A)-YFP pid-14* lines and the *pPID:PID-YFP pid-14* line or wild-type Arabidopsis (Col-0) at early developmental stages e.g. with respect to gravitropic growth, primary root length or rosette phenotype (Figure 1A-C, Figure S1A, B). Also, there was no clear difference between the flowering time of the tested lines (Figure 1C, Figure S1C), which showed a similar *PID* expression level (Figure 1D). A low percentage of the *pPID:PID(R→A)-YFP pid-14* or *pPID:PID-YFP pid-14* seedlings developed three cotyledons, a phenotype that was not linked to the R→A substitutions, but most likely to the promoter-cDNA-YFP construct design. The lack of an intron in the coding region of the *PID* gene probably altered the spatio-temporal expression, leading to insufficient expression in the embryo and thus to incomplete complementation of the *pid* mutant.

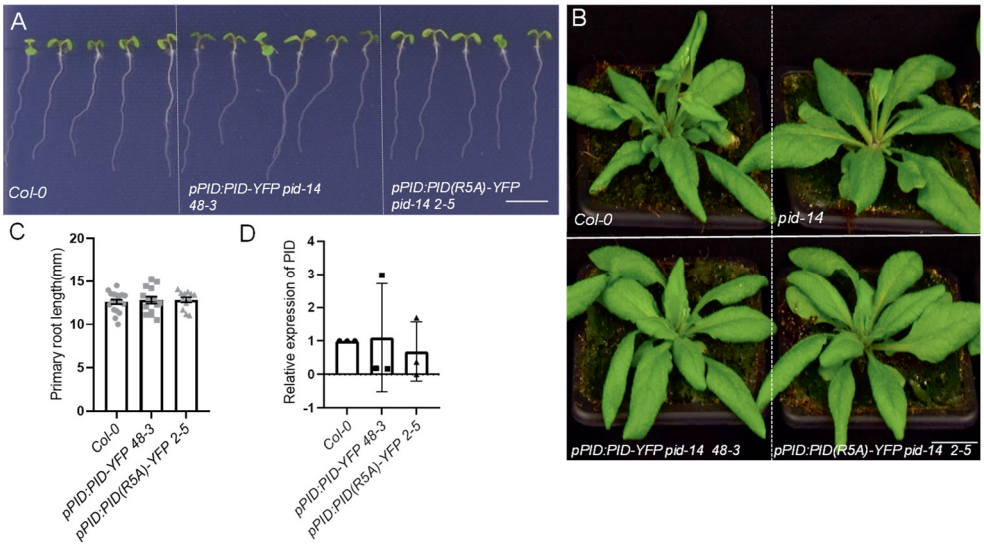

Figure 1. Seedlings and bolting plants of *pPID:PID(R5A)-YFP pid-14* lines show no obvious phenotypic differences from wild-type Arabidopsis (Col-0) or *pPID:PID-YFP pid-14* control lines. (A) 5-day-old seedlings of wild-type Arabidopsis (Col-0), and representative lines containing *pPID:PID-YFP* or *pPID:PID(R5A)-YFP* in the homozygous *pid-14* mutant background. **(B)** 6-week-

old bolting plants of wild-type Arabidopsis (Col-0), and representative lines containing *pPID:PID-YFP* or *pPID:PID(R5A)-YFP* in the homozygous *pid-14* mutant background. See also Figure S1. **(C)** Quantification of primary root length of 5-day-old seedlings (n = 11-14) in **(A). (D)** Quantitative RT-PCR analysis of PID expression for the lines presented in **(A)**. Bars in (**C** and **D**) represent means, error bars the SEM, and dots the values of the biological repeats. The experiment was repeated three times. A one-way ANOVA with Tukey's test was used to test for statistically significant differences. Size bar indicates 5 mm in **(A)**, 2 cm in **(B)**.

'Untouchable' PID leads to abnormal inflorescence phyllotaxis

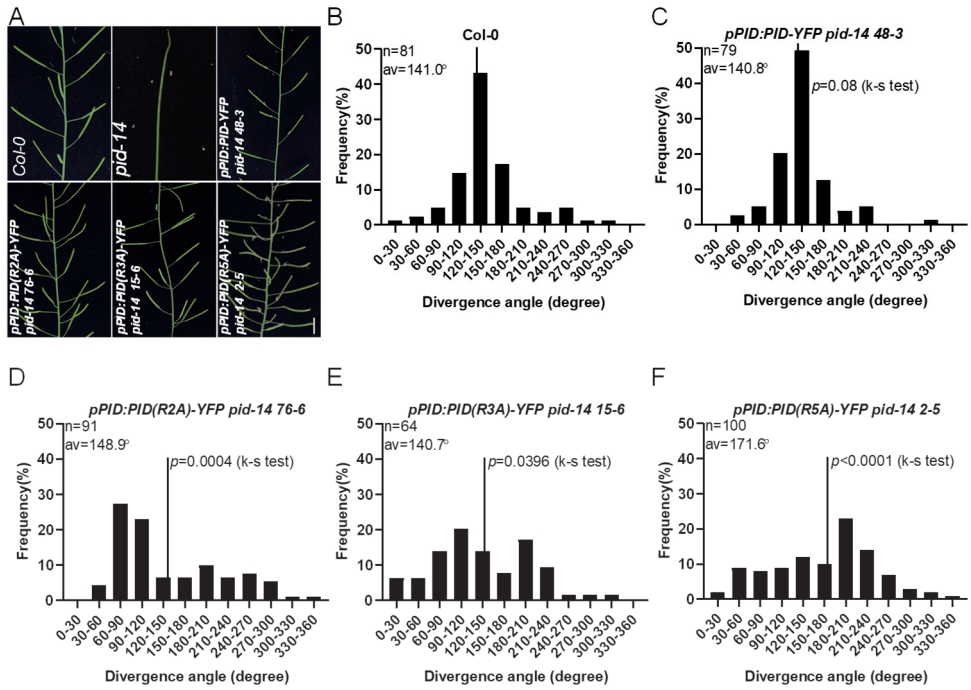

Figure 2. Expression of 'untouchable' PID versions in the *pid* mutant background leads to severe inflorescence phyllotaxis defects. (A) Representative inflorescences of 8-week-old wild-type Arabidopsis (Col-0) or *pid-14*, *pPID:PID-YFP pid-14* or *pPID:PID(R→A)-YFP pid-14* plants. **(B-F)** Distribution of divergence angles between two successive siliques along the inflorescences of wild-type Arabidopsis (Col-0) (**B**), *pPID:PID-YFP pid-14* **(C)**, *pPID:PID(R2A)-YFP pid-14* **(D)**, *pPID:PID(R3A)-YFP pid-14* **(E)** or *pPID:PID(R5A)-YFP pid-14* **(F)**. Divergence angles were classified into 12 classes of 30°, and the percentages per class over the total number measured (n) are indicated in each graph. The average (av) divergence angle is shown and indicated as black line in the graph. For each construct, inflorescences of at least five lines were measured. The Kolmogorov–Smirnov test showed significant difference between Col-0 wild type and *pPID:PID(R2A)-YFP pid-14 (p=0.0004)*, *pPID:PID(R3A)-YFP pid-14 (p=0.0396)* or *pPID:PID(R5A)-YFP pid-14 (p<0.0001).* Size bar in **(A)** indicates 1 cm.

Initial observations suggested that the *pPID:PID(R→A)-YFP* construct complemented the pin like inflorescence phenotype of the *pid-14* mutant. More close inspection of the *pPID:PID(R→A)-YFP pid-14* inflorescences, however, showed clear defects in the spiral phyllotaxis that is typically observed in inflorescences of wild-type Arabidopsis (Col-0) (Figure 2A, B). In the latter inflorescences and also in those of *pPID:PID-YFP pid-14* plants, successive flowers arose and diverged by average angles of 141° (n=81) and 140.8° (n=79), respectively, statistically approximating the so-called the 'golden' angle of 137.5°. In contrast, the flowers of the *pPID:PID(R→A)-YFP pid-14* plants initiated in a disordered, almost randomized, fashion, with average divergence angles significantly deviating from the golden angle, or with angle value frequencies that deviated from a normal distribution (Figure 2D-F). We did not observe a specific pattern in the deviations from the spiral phyllotaxis. The data suggests that the role of the PID CaM/CML interaction is to prevent randomized organ initiation and promote positioning of subsequent organ primordia at a regular distance leading to the 'golden' divergence angle that it typical for spiral phyllotaxis in Arabidopsis.

'Untouchable' PID causes simultaneous flower primordium initiation and increases the variation in IM size

The IM generates the inflorescence and is the major determinant of the final phyllotactic pattern. However, the divergence angle in spiral phyllotaxis can also be modulated by post-meristematic growth such as internode elongation or stem torsion (Byrne et al., 2003; Peaucelle et al., 2007; Landrein et al., 2013). To investigate the cause of the observed irregular inflorescence phyllotaxis in more detail, we partially dissected the inflorescences of wild-type Arabidopsis (Col-0) and the wild-type PID or 'untouchable' PID complemented lines (Figure 3A).

In wild-type plants, each flower was attached by its pedicel to a single node, and nodes were separated by an internode, of which the length decreased gradually with each higher position on the inflorescence stem. The *pPID:PID-YFP pid-14*

plants showed the same flower, node, internode pattern (Figure 2A, 3A). In contrast, in *pid-14* mutant lines expressing 'untouchable' PID we frequently observed short internodes in between two longer ones, coinciding with an aberrant divergence angle, or two or even more flowers with their pedicels attached to the same node (Figure 2A, 3A). In some cases, two flowers were attached via the same pedicel to a node, or via their own pedicel to the same node but at a divergence angle of 180°. These data indicates that the irregular inflorescence phyllotaxis is not caused by defects of internode growth, but rather by the irregular and sometimes simultaneous initiation of flower primordia at the IM, subsequently causing irregular internode lengths.

Figure 3. 'Untouchable' PID expression leads to simultaneous flower primordium initiation. (A) Partially dissected inflorescences of 8-week-old wild-type Arabidopsis (Col-0) or *pPID:PID-YFP pid-14*, *pPID:PID(R2A)-YFP pid-14*, *pPID:PID(R3A)-YFP pid-14* or *pPID:PID(R5A)-YFP pid-14* plants. White arrows indicate positions where flower primordia were simultaneously initiated. **(B)** Subsequent fruits and flowers picked from the top part of a wild-type Arabidopsis (Col-0) inflorescence, showing a nice developmental series (upper panel), and clusters of co-initiated flowers picked from the top of *pPID:PID(R2A)-YFP pid-14*, *pPID:PID(R3A)-YFP pid-14* or *pPID:PID(R5A)-YFP pid-14* inflorescences. Size bar indicates 2 mm in **(A)**.

To further confirm these results, we checked the developmental stages of subsequent fruits and flowers picked from the top part of an inflorescence. In wild-type Arabidopsis (Col-0) or the *pid-14* mutant complemented with wild-type PID

(*pPID:PID-YFP pid-14*) we observed a perfect developmental series, with each subsequent fruit or flower being at an earlier developmental stage, reflecting their sequential and regular timing of initiation at the IM (Figure 3B). In contrast, when we did the same for the *pid-14* mutants complemented with the 'untouchable' PID versions (*pPID:PID(R→A)-YFP pid-14*), we observed clusters of the flowers at the same developmental stage, indicating that they were simultaneously initiated at the IM (Figure 3A, B).

To validate that flower primordia were initiated simultaneously and to gain more mechanistic insight, we studied the anatomy of the IMs by scanning electron microscopy (SEM). At Col-0 IMs, flower primordia were initiated gradually in a regular clockwise or counter-clockwise spiral pattern (Figure 4A). The order from the youngest to the oldest primordium could be easily identified based on their developmental stage, with a divergence angle between successive primordia close to 137.5°, the so-called "golden angle" (Jean and Barab, 1998; Figure 4A). The IMs of *pid-14* mutant plants generally failed to initiate flower primordia organs and thus formed the typical 'pin-like' apical structures (Figure 4B). When the *pid-14* mutant was complemented with wild-type PID (*pPID:PID-YFP pid-14*), the IM showed the normal spiral pattern of primordium initiation that was also observed in Col-0 (Figure 4C). Markedly, the IMs of the *pid-14* mutant complemented with 'untouchable' PID versions (*pPID:PID(R→A)-YFP pid-14*) displayed a more random and variable pattern of flower primordium initiation, with simultaneous primordium initiation occurring frequently (Figure 4D-F). In some cases, two or even more primordia were initiated at one site of the SAM (e.g., P2? and P4? in Figure 4D and E), in line with the observed clusters of flowers and fruits (Figure 2A, Figure 3B).

Irregular phyllotactic patterns and simultaneous primordium initiation have previously been associated with an increased meristem size (Landrein et al., 2015; Yin, 2021). We used the SEM images to measure and compare the size of the IM of wild-type versus the *pid-14* complemented lines. Unexpectedly, the average IM

size of *pPID:PID(R→A)-YFP pid-14* plants was not significantly larger than that of wild-type Arabidopsis or *pPID:PID-YFP pid-14* plants, but we did observe a significant increase in the variation in size of the individual IMs (Figure 4G).

Together, our data shows that the Ca^{2+}-dependent regulation of PID activity by the CaM/CMLs is required to perfectly arrange newly formed organs by generating the regular spiral phyllotaxis and to prevent the simultaneous initiation of flower primordia at the IM. As PID function is not directly linked to the regulation of meristem size, we hypothesize that the latter is an indirect consequence of the phyllotaxis defects.

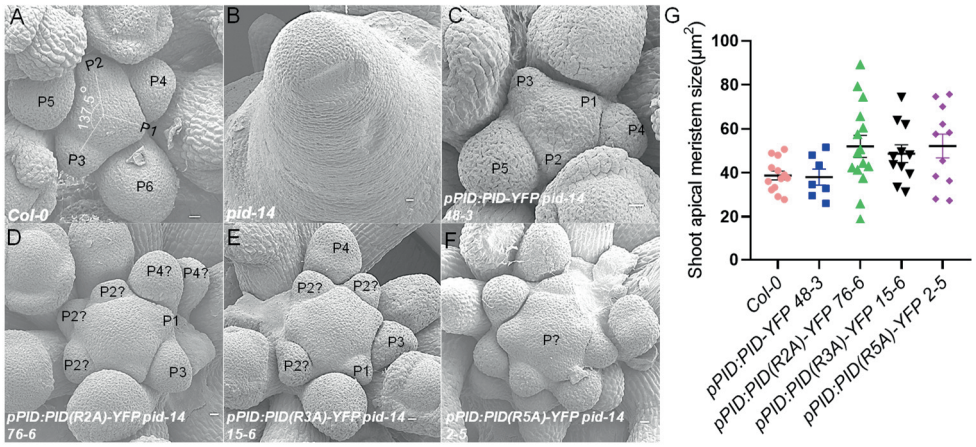

Figure 4. 'Untouchable' PID leads to simultaneous flower primordium initiation and increases the variation in IM size. (**A-F**) Scanning electron microscopy images of dissected inflorescence meristems of 7-week-old wild-type Arabidopsis (Col-0) (**A**) or *pid-14* (**B**), *pPID:PID-YFP pid-14* (**C**), *pPID:PID(R2A)-YFP pid-14* (**D**), *pPID:PID(R3A)-YFP pid-14* (**E**) or *pPID:PID(R5A)-YFP pid-14* (**F**) plants. The flower primordia are indicated with a P and the number indicates the developmental order from young to older. P? in (**F**) indicates that for this IM it was difficult to stage the different primordia. (**G**) Quantitative analysis of IM size (in μm^2) of the plant lines presented in (**A**). Dots, squares, triangles or diamonds indicate the sizes of individual IMs, the black line indicates the average size. A one-way ANOVA with Tukey's test showed no significant difference in the average IM size between plant lines. However, an F-test indicated a significant increase in the variation in IM sizes in line *pPID:PID(R2A)-YFP pid-14* 76-6 (p=0.0008), *pPID:PID(R3A)-YFP pid-14* 15-6 (p=0.028), or *pPID:PID(R5A)-YFP pid-14* 2-5 (p=0.023), compared to Col-0, but not in line *pPID:PID-YFP pid-14* 48-3 (p=0.192). Size bar in (**A-F**) indicates 10 µm.

'Untouchable' PID leads to mis-positioning of PIN-generated auxin maxima in the IM.

It is well-established that auxin maxima generated by PIN1-driven PAT are the initiation points of flower primordia in the IM (Kuhlemeier and Reinhardt, 2001; Reinhardt et al., 2003; Jonsson et al., 2006; Sassi and Vernoux, 2013). More recent microscopy analysis combined with computational modelling suggests that these maxima are not fixed in space, but rather are waves of high auxin travelling through the IM in a centrifugal (outward directed) manner. The duration of exposure to high auxin was suggested to be the decisive trigger for primordium initiation (Galvan-Ampudia et al., 2020). Like PIN1, also PID has an important role in this process, as it allows the generation of auxin maxima by directing apical PIN1 localization, resulting in upward PAT through the epidermis of the IM (Friml et al., 2004; Huang et al., 2010).

In both wild-type Arabidopsis (Col-0) and the *pid-14* mutant complemented with wild-type PID (*pPID:PID-YFP pid-14*), the *pDR5:GFP* reporter indicated three strong auxin response maxima marking the positions of incipient primordium i(1) and primordia P1 and P2, respectively. In addition, weaker signals were observed colocalizing with the initiated primordia P3, P4 and P5, respectively (Figure 5A, C). The developmental order of the primordia, as indicated by the auxin maxima, was clear and they appeared at a divergence angle typical for the spiral phyllotaxis in Arabidopsis. In the *pid-14* loss-of-function mutant, no auxin response maxima were observed in the IM (Figure 5B), in line with the rootward/basal polarity of PIN1 (Figure 5F, J) and the absence of flower primordia on the pin-like inflorescences of this mutant (Figure 4B). In the *pid-14* mutant lines complemented with 'untouchable' PID (*pPID:PID(R5A)-YFP pid-14*) we observed a more dispersed distribution of auxin response maxima in the IM (Figure 5D). At least 6 auxin response maxima were observed, which is significantly more than the 3 to 4 observed in wild-type Arabidopsis (Figure 5M). Moreover, the developmental order of the incipient primordia that are marked by these auxin maxima could not be distinguished, as a clear spiral pattern of incipient primordia was absent. These results indicate that the main role of the Ca^{2+}-dependent regulation of PID kinase

activity is to control the position of primordium initiation by limiting the number of auxin response maxima in the IM.

As *PIN1* expression is auxin responsive and PID regulates PIN1 polarity, we compared *PIN1* expression and PIN1 polarity in Arabidopsis wild-type with that in the *pid-14* mutant or the different complemented lines. In wild-type Arabidopsis or in *pid-14* mutant lines complemented with wild-type PID *PIN1* was expressed throughout the L1 layer of the IM, but most strongly in flower primordia P1 to P3, where its polar localization converged towards the primordium tip (Figure 5E, G). Conversely, in the *pid-14* loss-of-function mutant we observed weaker but even *PIN1* expression in the L1 layer of the pin-like IM and predominant rootward/basal localisation of the protein (Figure 5F, J). No PIN1 convergence points were observed, in line with the absence of flower primordia (Figure 5F, J). In *pid-14* mutant lines complemented with 'untouchable' PID, PIN1 was also expressed throughout the L1 layer of the IM, with stronger expression at sites of incipient and young primordia. As observed for the *pDR5:GFP* reporter, the number of PIN1 convergence points was markedly higher than in wild-type IMs (Figure 5H). The confocal images did not allow us to detect obvious differences in PIN1 polarity between wild-type Arabidopsis or wild-type PID complemented lines and the 'untouchable' PID complemented lines. Confocal sections of IMs below the L1 layer showed 3-4 stronger signals corresponding to the convergence points in wild-type Arabidopsis or wild-type PID complemented lines, representing the pro-vascular cells with rootward-oriented PIN1 that will later form the vascular tissue connecting the newly formed organs to the existing vascular system of the plant. In the 'untouchable' PID complemented lines we observed 6 to 7 signals (Figure 5L), in line with the increase of the number of *pDR5:GFP* signals and PIN1 marked convergence points (Figure 5M).

These results indicate that, the altered auxin distribution in the IM is driven by the marked change of PIN1 expression pattern.

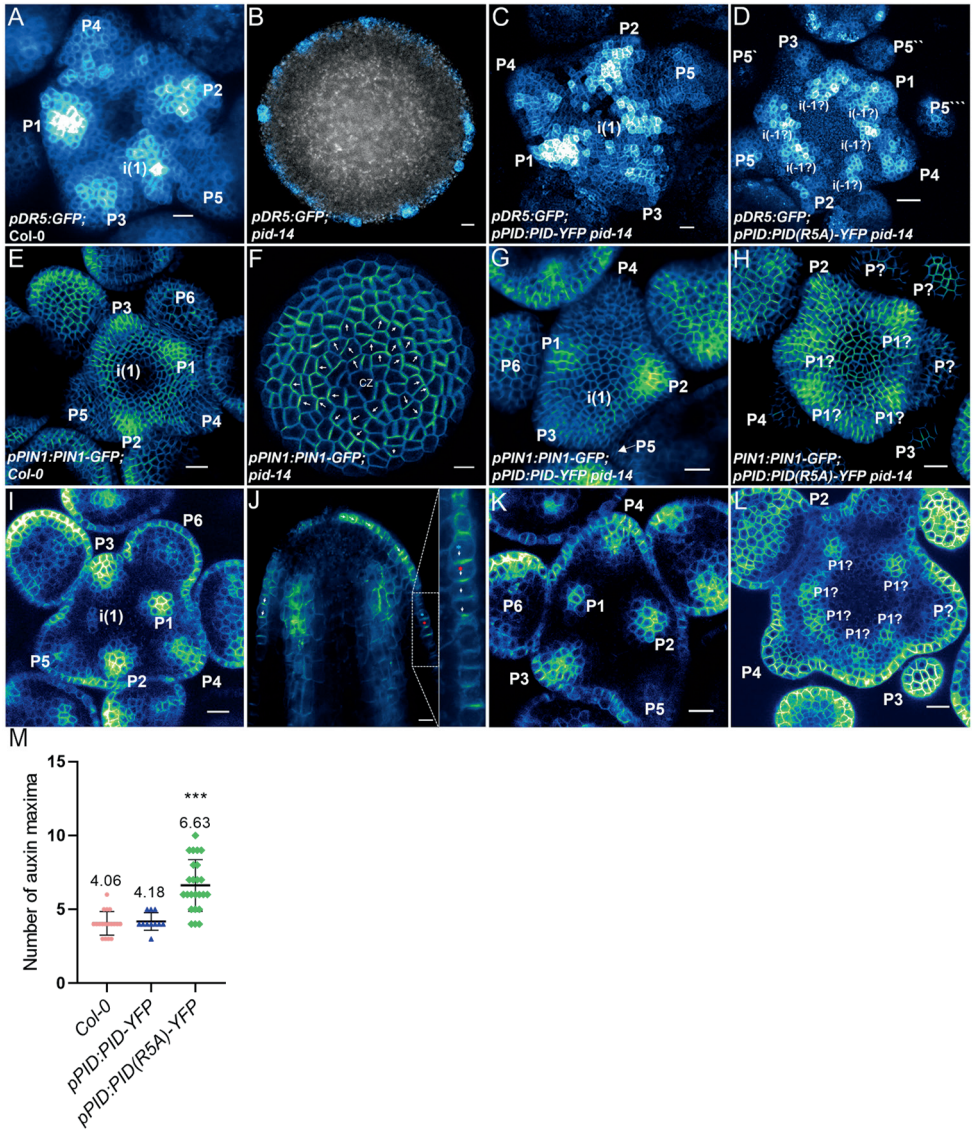

Figure 5. 'Untouchable' PID results in more auxin response maxima and in mis-positioned PIN1 convergence points. (**A-D**). Expression of *pDR5:GFP* in Col-0 **(A)**, *pid-14* **(B)** and 'untouchable' PID mutant complementary line: *pPID:PID-YFP* **(C)** or *pPID:PID R5A-YFP* (**D)** in the homozygous *pid-14* mutant background. (**E-H**) 3D reconstructed top view of Arabidopsis SAMs showing the expression of *PIN1:PIN1-GFP* in Col-0 (**E**), *pid-14* **(F)**, and lines containing *pPID:PID-YFP* **(G)**, or *pPID:PID R5A-YFP* **(H)** in the homozygous *pid-14* mutant background. Confocal stacks obtained from *pPIN1:PIN1-GFP* expressing plants were converted into 3D. **(I-L)** Horizontal or longitudinal section view in **(E-H)** respectively. **(M)** Quantitative analysis of auxin maxima in the SAM of the plants presented in **(A, C, D).** One-way ANOVA with Tukey's test showed significant

difference between Col-0 and *pPID:PID R5A-YFP* (***p<0.001), but not with line *pPID:PID-YFP*. White letter P stands for primordia, the number indicates the developmental order of the primordia. CZ: central zone of SAM. i: incipient primordia. White arrow indicates the PIN1 polarity. Stars in same color indicate the same cell. Size bar indicates 10 nm in **(A-D)** and 20 nm in **(E-L)**.

Discussion

Plant organs are repetitively generated at the SAM in a precise spatio-temporal pattern, known as phyllotaxis (Yin, 2021). The phytohormone auxin and its polar transport play a pivotal role in organogenesis at the SAM. Accumulating evidence suggests that calcium signalling is involved in modulating auxin responses and PAT (Dela Fuente and Leopold, 1973; Lee et al., 1984; Plieth and Trewavas, 2002; Toyota et al., 2008). In this study, we found that Ca^{2+}-dependent binding of CaM/CMLs regulates the activity of the PID kinase, an important regulator of PAT, and modulates the distribution of PIN-driven auxin maxima and patterns phyllotaxis at the SAM.

The CaM/CML-PID interaction confirms the importance of Ca^{2+} signalling in phyllotaxis

It is well established that auxin and its polar transport are necessary and sufficient for organ formation at the SAM. This is supported by the findings that inhibition of PAT, either by treatment with the PAT inhibitor N-1-naphthylphthalamic acid (NPA) or by mutations in PIN1 or PID, terminates organ initiation at the flanks of the SAM and results in the formation of pin-like inflorescences lacking flowers (Okada et al., 1991; Bennett et al., 1995; Vernoux et al., 2000; Reinhardt et al., 2000; Bohn-Courseau, 2010). Moreover, application of exogenous auxin to these pin-like apices has been shown to restore organ initiation, indicating that they are deprived of auxin and that auxin is sufficient for organ initiation at the IM (Reinhardt et al., 2000; Reinhardt et al., 2003). PIN1 is predominantly expressed in the L1 layer and in the provascular cells in the IM (Figure 5; Benková et al., 2003; Reinhardt et al., 2003; Heisler et al., 2005), where it directs auxin flux through its highly dynamic expression and polarity patterns, forming convergence points that trigger

primordium initiation by generating auxin maxima in a regular pattern (Figure 5A and E; Heisler et al., 2005; Bhatia and Heisler, 2018; Galvan-Ampudia et al., 2020). How this PIN1 dynamics is coordinated to form these convergences points in a regular pattern was still not fully understood. Several lines of evidence indicate that both exogenous and endogenous signals triggering rapid changes in $[Ca^{2+}]_{cyt}$ are involved (Zhang et al., 2011; Goh et al., 2012; Shih et al., 2015; Li et al., 2019). Our findings now provide a clear molecular basis connecting Ca2+ signaling to the dynamic action of the two key players in phyllotaxis, the PIN1 auxin efflux carriers and the PID protein kinase regulating their polarity and activity.

The Ca2+-dependent regulation of PID activity integrates auxin and mechanical stress signaling during phyllotactic patterning.

The dynamic PIN1 convergence patterns are the result of feedback between auxin and the expression and polarity of PIN1 on the one hand, and mechanical stress in the IM caused by the continuous initiation and outgrowth of new organs on the other (Smith et al., 2006; Heisler et al., 2010; Bhatia et al., 2016; Kareem et al., 2022).

New organs in the meristem are initiated through accumulation of auxin at specific sites in the peripheral zone, and accumulation of auxin starting from the earlier steps of organ initiation (Vernoux et al., 2011; Brunoud et al., 2012). Mechanisms acting downstream of auxin that regulated PIN1 convergences have been reported, for example the AUXIN RESPONSE FACTOR 5/MONOPTEROS (ARF5/MP) (Bhatia et al., 2016; Garrett et al., 2012; Fal et al., 2017). MP positions the auxin-responsive *PIN1* expression, thereby facilitating a positive feedback loop that results in periodic organ formation (Bhatia et al., 2016). Disruption of MP-mediated auxin signalling or the auxin positive feedback loop causes ectopic PIN1 expression, thereby disturbing the position of auxin maxima leading to altered floral phyllotaxis (Garrett et al., 2012; Fal et al., 2017).

The initiation of primordia at the SAM is associated with the presence of high mechanical stress levels (Lyndon, 1998; Uyttewaal et al., 2012). Of the genes encoding CaM/CML sensor proteins, particularly *CaM1/TCH1* and *CML12/TCH3* are of interest, as these genes have been shown to be highly upregulated in response to mechanical stress and auxin and mechanical stress, respectively (Braam and Davis, 1990; Braam et al., 1997; McCormack et al., 2005; Chapter 2). Based on these findings and the results presented in this chapter we hypothesize that the continuous organ initiation and growth at the SAM leads to dynamic local increases in mechanical stress that trigger elevation of $[Ca^{2+}]_{cyt}$ together with an increased Ca^{2+} sensing capacity by in the elevated expression of *CaM/CML* genes. Binding of Ca^{2+} activates the CaM/CMLs (Ca^{2+}-CaM/CMLs), which in turn inhibit PID activity by binding to this kinase, leading to reduced PIN1 phosphorylation and resulting in local changes in PIN1 polarity and activity. This local inactivation of PIN1 is required to pin point the position of the next PIN1 convergence point directing auxin maxima-induced organ initiation (Figure 6). In the *pid* mutant lines expressing 'untouchable' PID, this controlled positioning as a result of the feedback of auxin and mechanical stress on PAT processes in the SAM is absent, leading to mispositioning and erroneous timing of organ initiation. Phenotypes of the Arabidopsis *katanin1* mutant provide support for this hypothesis. KATANIN1 (KTN1) is a microtubule severing protein, and the *ktn1* mutant is defective in cortical microtubule bundling, which prevents oriented cellulose deposition (Bichet et al., 2001; Burk and Ye, 2002), resulting in a reduced global response to mechanical stress at the SAM (Uyttewaal et al., 2012) and thus in a perturbed phyllotaxis (Jackson et al., 2019). Where exactly in the SAM auxin feedback and mechanical stress come together to decrease PID activity still needs to be established. The most likely position is just distal to where the new convergence point should be established. As the reduction in PID activity is likely to be very transient, changes in PIN polarity may not reveal this position. Instead, the use of

more recently developed Ca^{2+} reporters combined with reporters that show the PID-CaM/CML interaction itself may provide more insight into this matter.

In summary, our results reveal a novel mechanism by which Ca^{2+}-dependent control of PID activity through the CaM/CML sensor proteins plays a crucial role in coordinating auxin distribution at the SAM and maintaining the normal phyllotaxis pattern through regulation of PIN1 convergence points (Figure 6). In the absence of PID, basal polarity of PIN1 deprives the SAM of auxin, resulting in pin-like inflorescences that lack organ initiation. When the Ca^{2+}-dependent control of PID activity is removed, this leads to mispositioning of primordium initiation and often to co-initiation of primordia, resulting in inflorescences with aberrant phyllotactic patterns and more flowers compared to wild type (Figure 6).

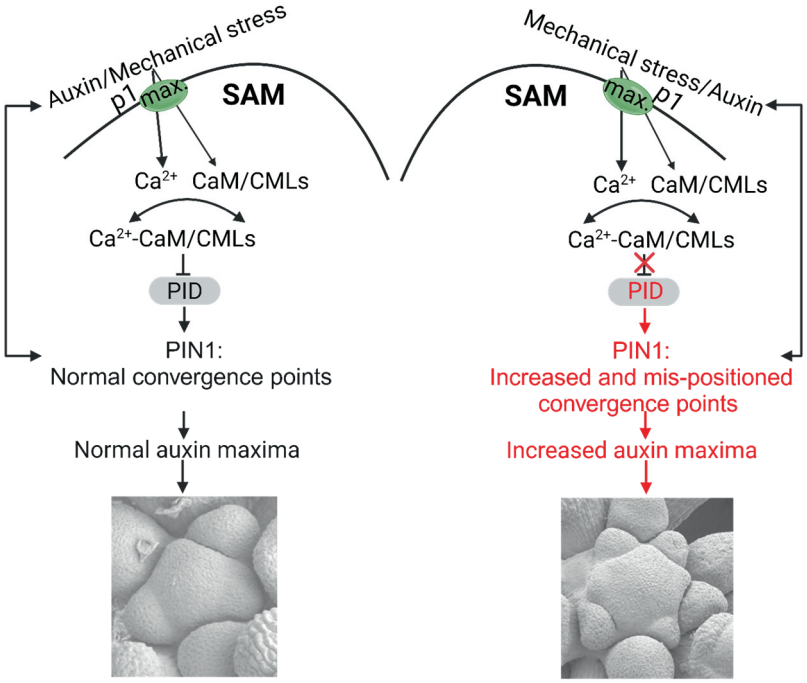

Figure 6. A model showing the involvement of CaM/CMLs-PID complex in patterning phyllotaxis. Mechanical stress and auxin induce the high expression of the major Ca^{2+} sensors *CaM/CMLs* and trigger elevation of $[Ca^{2+}]_{cyt}$, which activates the CaM/CMLs (Ca^{2+}-CaM/CMLs). Ca^{2+}-CaM/CMLs suppresses PID kinase activity and thereby affect the expression pattern of its phosphorylation target, PIN1 protein. Expression pattern of PIN1 then instructs the auxin distribution at the SAM thus patterning phyllotaxis.

Material and Methods

Arabidopsis lines and plant growth

All Arabidopsis lines are in the Col-0 background. The *pid-14* loss-of-function mutant and the *pPIN1:PIN1-GFP* and *pDR5:GFP* reporter lines were described previously (Friml et al., 2004; Benkova et al., 2003). Arabidopsis transgenic lines in the homozygous *pid-14* mutant background, *pPID:PID-YFP pid-14*, *pPID:PID(R2A)-YFP pid-14*, *pPID:PID(R3A)-YFP pid-14* and *pPID:PID(R5A)-YFP pid14* are described in Chapter 3.

For the seed germination on sterile medium, seeds were surface sterilized by incubating 1 min in 70% ethanol and 10 min in bleach solution containing 1% chlorine. Sterilized seeds were subsequently washed three times with sterile dH_2O, kept in the dark at 4°C for two days for vernalization and germinated on vertical plates containing 0.5× Murashige and Skoog (1/2 MS) Duchefa medium with 0.05% MES, 1% Daishin agar (Duchefa) and 1% sucrose at 22 °C and 16 hours photoperiod. Plants grown on soil were cultured at 21°C, 16 hours photoperiod and 70% relative humidity.

Phenotypic analysis and microscopy

Seedlings on plates, soil grown plants and inflorescence details were photographed with a Nikon D5300 camera. The primary root length of seedlings was measured with ImageJ (Fiji) and analysed with GraphPad Prism 5.

The phyllotactic pattern was assessed on fully grown inflorescences of 8-week-old plants. Divergence angles were measured as described in Peaucelle et al. (2007). IMs were dissected from inflorescences of 5-week-old plants and placed with the bottom internode in a drop of 1% low melting point agarose and observed with a Nikon AX Confocal microscope using a 40x long working distance water dipping objective. The fluorescent signal from the *pDR5:GFP* or *pPIN1:PIN1-GFP* reporters was monitored using an argon laser for excitation at 488 nm and a 505-

530nm band pass emission filter. Images were processed using Image J. For scanning electron microscopy (SEM) imaging, IMs were dissected from inflorescences of 7-week-old plants and fixed in 2% paraformaldehyde (PFA) and 1% glutaraldehyde in 1× phosphate-buffer saline (PBS) for two hours at 21 °C and subsequently overnight at 4 °C. Fixed IMs were washed twice with 1× PBS and dehydrated using an acetone series (70%, 80%, 90%, 100%) under vacuum. The samples were subsequently transferred to a Bal-Tec CDP030 critical point drier, where the acetone was replaced by liquid carbon dioxide. IMs were fixed to stubs and sputter coated with gold using SEM Coating unit 5100 (Polaron Equipment Ltd.). Gold was discharged by admitting pressurized argon in a low vacuum environment. Coated IMs were kept in dry under vacuum and were imaged with a JEOL SEM 6400 scanning electron microscope.

The size of IMs was measured using scanning electron microscopy (SEM) SAM images with the method as described in (Shi et al., 2018), the number of auxin maxima were counted using confocal microscope images. All date were analyzed and plotted into graphs in GraphPad Prism 8.

RNA extraction and RT-PCR

Vertically grown 5-day-old seedlings were collected and total RNA was extracted using the NucleoSpin RNA Plant kit (Macherey Nagel, #740949). Reverse transcription (RT) was performed using the RevertAid Reverse Transcription Kit (Thermo Scientific™, #K1691). qRT-PCR was performed in the CFX96 Touch™ Real-Time PCR Detection System (Bio-Rad) using TB Green® Premix Ex Taq™ II (Tli RNase H Plus) (Takara, #RR820B). primers used are: PP2A-3-qRT-FP: GATGGATACAACTGGGCTCACG3; PP2A-3-qRT-RP: TCGGTGCTGGTTCAAACTGG3; PID-qRT-FP: ATTTACACTCTCTCCGTCATAGACAAC3; PID-qRT-RP: ACATGTGTAGATATTCTAACGCCACTA

Accession numbers

Arabidopsis Genome Initiative locus identifiers for the genes mentioned are as follows: CML12/TCH3 (At2g41100), PID (At2g34650), PIN1(AT1G73590)

Acknowledgements

The authors would like to thank Gerda Lamers and Joost Willemse for their help with the microscopy, Ward de Winter and Jan Vink for help with medium, tissue culture and plant caretaking. This author was supported by the China Scholarship Council.

Author contribution

Remko Offringa, Xiaoyu Wei designed the experiments, Xiaoyu Wei performed the experiments and data analysis, Xiaoyu Wei and Remko Offringa wrote and finalized the Chapter.

Supplementary data:

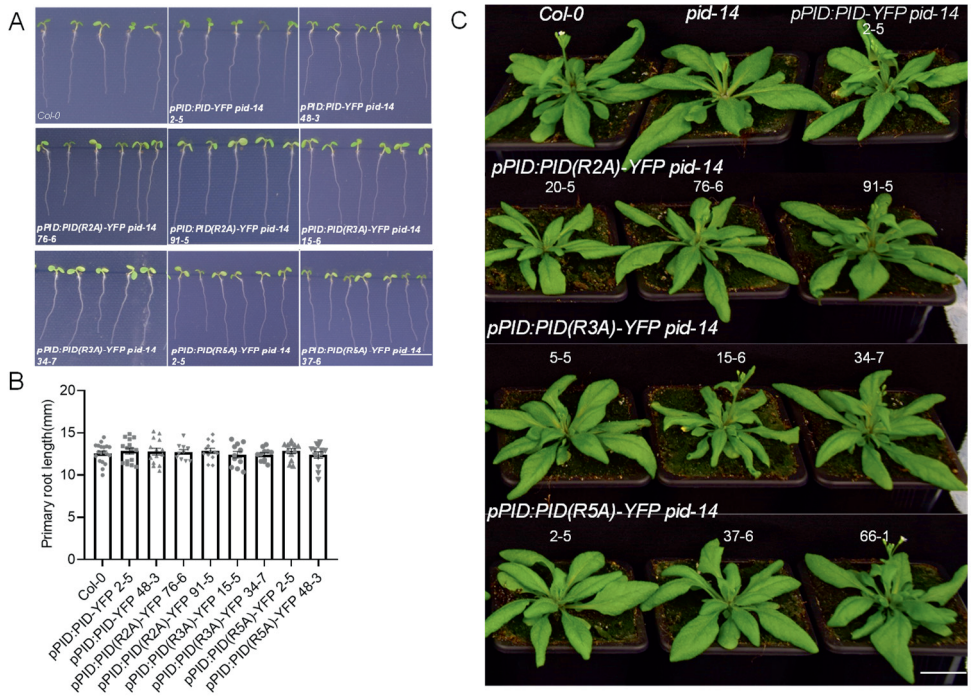

Figure S1. Seedlings and bolting plants of *pPID:PID(R→A)-YFP pid-14* lines show no obvious phenotypic differences from wild-type Arabidopsis (Col-0) or *pPID:PID-YFP pid-14* control lines. . (**A**) 5-day-old seedlings of wild-type Arabidopsis (Col-0) or *pPID:PID-YFP pid-14*, *pPID:PID(R2A)-YFP pid-14, pPID:PID(R3A)-YFP pid-14* or *pPID:PID(R5A)-YFP pid-14* plants. **(B)** Quantification of primary root length of 5-day-old seedlings in **(A)**. Results of a representative triplicate experiment are shown. Bars represent means, error bars the SEM, and dots the values of the individual seedlings (n=11-14). A one-way ANOVA with Tukey's test detected no significant differences between the tested plant lines. **(C)** 6-week-old bolting plants of wild-type Arabidopsis (Col-0) or or *pPID:PID-YFP pid-14*, *pPID:PID(R2A)-YFP pid-14, pPID:PID(R3A)-YFP pid-14* or *pPID:PID(R5A)-YFP pid-14* plants. Size bar in indicates 5 mm in **(A)**, 2 cm in **(B)**.

Reference:

Adamowski, M., & Friml, J. (2015). PIN-dependent auxin transport: action, regulation, and evolution. Plant Cell 27: 20–32.

Barbosa, I. C., Hammes, U. Z., & Schwechheimer, C. (2018). Activation and polarity control of PIN-FORMED auxin transporters by phosphorylation. Trends Plant Sci. 23: 523-538.

Benjamins, R., Ampudia, C.S., Hooykaas, P.J., & Offringa, R. (2003). PINOID-mediated signaling involves calcium-binding proteins. Plant Physiol. 132: 1623-1630.

Benková, E., Michniewicz, M., Sauer, M., Teichmann, T., Seifertová, D., Jürgens, G., & Friml, J. (2003). Local, efflux-dependent auxin gradients as a common module for plant organ formation. Cell 115: 591-602.

Benková, E., Michniewicz, M., Sauer, M., Teichmann, T., Seifertová, D., Jürgens, G., & Friml, J. (2003). Local, efflux-dependent auxin gradients as a common module for plant organ formation. Cell 115: 591-602.

Bennett, S. R., Alvarez, J., Bossinger, G., & Smyth, D. R. (1995). Morphogenesis in *pinoid* mutants of Arabidopsis thaliana. Plant J. 8: 505-520.

Bhatia, N., & Heisler, M. G. (2018). Self-organizing periodicity in development: organ positioning in plants. Development 145: dev149336.

Bhatia, N., Bozorg, B., Larsson, A., Ohno, C., Jönsson, H., & Heisler, M. G. (2016). Auxin acts through MONOPTEROS to regulate plant cell polarity and pattern phyllotaxis. Curr. Biol. 26: 3202-3208.

Bichet, A., Desnos, T., Turner, S., Grandjean, O., & Höfte, H. (2001). BOTERO1 is required for normal orientation of cortical microtubules and anisotropic cell expansion in Arabidopsis. Plant J. 25: 137-148.

Bohn-Courseau, I. (2010). Auxin: a major regulator of organogenesis. C. R. Biol. 333: 290-296.

Braam, J., & Davis, R. W. (1990). Rain-, wind-, and touch-induced expression of calmodulin and calmodulin-related genes in Arabidopsis. Cell 60: 357-364.

Braam, J., Sistrunk, M. L., Polisensky, D. H., Xu, W., Purugganan, M. M., Antosiewicz, D. M., ... & Johnson, K. A. (1997). Plant responses to environmental stress: regulation and functions of the Arabidopsis TCH genes. Planta 203: S35-S41.

Brunoud, G., Wells, D. M., Oliva, M., Larrieu, A., Mirabet, V., Burrow, A. H., ... & Vernoux, T. (2012). A novel sensor to map auxin response and distribution at high spatio-temporal resolution. Nature 482: 103-106.

Burk, D. H., & Ye, Z. H. (2002). Alteration of oriented deposition of cellulose microfibrils by mutation of a katanin-like microtubule-severing protein. Plant Cell 14: 2145-2160.

Byrne, M. E., Groover, A. T., Fontana, J. R., & Martienssen, R. A. (2003). Phyllotactic pattern and stem cell fate are determined by the Arabidopsis homeobox gene BELLRINGER. Development 17: 3941-50.

Dela Fuente, R.K., and Leopold, A.C. (1973). A role for calcium in auxin transport. Plant Physiol. 51: 845-847.

Dhonukshe, P., Huang, F., Galvan-Ampudia, C. S., Mähönen, A. P., Kleine-Vehn, J., Xu, J., ... & Offringa, R. (2010). Plasma membrane-bound AGC3 kinases phosphorylate PIN auxin carriers at TPRXS (N/S) motifs to direct apical PIN recycling. Development 137: 3245-3255.

Dory, M., Hatzimasoura, E., Kállai, B. M., Nagy, S. K., Jäger, K., Darula, Z., ... & Dóczi, R. (2018). Coevolving MAPK and PID phosphosites indicate an ancient environmental control of PIN auxin transporters in land plants. FEBS Lett. 592: 89-102.

Fal, K., Liu, M., Duisembekova, A., Refahi, Y., Haswell, E. S., & Hamant, O. (2017). Phyllotactic regularity requires the Paf1 complex in Arabidopsis. Development 144: 4428-4436.

Friml, J., Vieten, A., Sauer, M., Weijers, D., Schwarz, H., Hamann, T., ... & Jürgens, G. (2003). Efflux-dependent auxin gradients establish the apical–basal axis of Arabidopsis. Nature 426: 147-153.

Friml, J., Yang, X., Michniewicz, M., Weijers, D., Quint, A., Tietz, O., ... & Offringa, R. (2004). A PINOID-dependent binary switch in apical-basal PIN polar targeting directs auxin efflux. Science 306: 862-865.

Furutani, M., Nakano, Y., & Tasaka, M. (2014). MAB4-induced auxin sink generates local auxin gradients in Arabidopsis organ formation. Proceedings of the National Academy of Sciences 111: 1198-1203.

Galvan-Ampudia, C. S., Cerutti, G., Legrand, J., Brunoud, G., Martin-Arevalillo, R., Azais, R., ... & Vernoux, T. (2020). Temporal integration of auxin information for the regulation of patterning. Elife 9: e55832.

Galvan-Ampudia, C. S., Cerutti, G., Legrand, J., Brunoud, G., Martin-Arevalillo, R., Azais, R., ... & Vernoux, T. (2020). Temporal integration of auxin information for the regulation of patterning. Elife 9: e55832.

Garrett, J. J., Meents, M. J., Blackshaw, M. T., Blackshaw, L. C., Hou, H., Styranko, D. M., ... & Schultz, E. A. (2012). A novel, semi-dominant allele of

MONOPTEROS provides insight into leaf initiation and vein pattern formation. Planta 236: 297-312.

Goh, C. S., Lee, Y., & Kim, S. H. (2012). Calcium could be involved in auxin-regulated maintenance of the quiescent center in the Arabidopsis root. J. Plant Biol. 55: 143-150.

Heisler, M. G., Hamant, O., Krupinski, P., Uyttewaal, M., Ohno, C., Jönsson, H., ... & Meyerowitz, E. M. (2010). Alignment between PIN1 polarity and microtubule orientation in the shoot apical meristem reveals a tight coupling between morphogenesis and auxin transport. PLoS Biol. 8: e1000516.

Heisler, M. G., Ohno, C., Das, P., Sieber, P., Reddy, G. V., Long, J. A., & Meyerowitz, E. M. (2005). Patterns of auxin transport and gene expression during primordium development revealed by live imaging of the Arabidopsis inflorescence meristem. Curr. Biol. 15: 1899-1911.

Huang, F., Kemel Zago, M., Abas, L., van Marion, A., Galván-Ampudia, C. S., & Offringa, R. (2010). Phosphorylation of conserved PIN motifs directs Arabidopsis PIN1 polarity and auxin transport. Plant Cell 22: 1129-1142.

Jackson, M. D., Duran-Nebreda, S., Kierzkowski, D., Strauss, S., Xu, H., Landrein, B., ... & Bassel, G. W. (2019). Global topological order emerges through local mechanical control of cell divisions in the Arabidopsis shoot apical meristem. Cell Syst. 8: 53-65.

Jean, R. V., & Barab, D. (1998). Symmetry in plants . J. Plant Physiol. 157: 356.

Jia, W., Li, B., Li, S., Liang, Y., Wu, X., Ma, M., ... & Wang, Y. (2016). Mitogen-activated protein kinase cascade MKK7-MPK6 plays important roles in plant development and regulates shoot branching by phosphorylating PIN1 in Arabidopsis. PLoS Biol. 14: e1002550.

Jönsson, H., Heisler, M. G., Shapiro, B. E., Meyerowitz, E. M., & Mjolsness, E. (2006). An auxin-driven polarized transport model for phyllotaxis. Proc. Natl. Acad. Sci. U.S.A. 103: 1633-1638.

Kareem, A., Bhatia, N., Ohno, C., & Heisler, M. G. (2022). PIN-FORMED1 polarity in the plant shoot epidermis is insensitive to the polarity of neighboring cells. Iscience 25: 105062.

Keinath, N. F., Waadt, R., Brugman, R., Schroeder, J. I., Grossmann, G., Schumacher, K., & Krebs, M. (2015). Live cell imaging with R-GECO1 sheds light on flg22-and chitin-induced transient [Ca2+] cyt patterns in Arabidopsis. Mol. Plant 8: 1188-1200.

Kleine-Vehn, J., Wabnik, K., Martiniere, A., Łangowski, Ł., Willig, K., Naramoto, S., ... & Friml, J. (2011). Recycling, clustering, and endocytosis

jointly maintain PIN auxin carrier polarity at the plasma membrane. Mol. Syst. Biol. 7: 540.

Kuhlemeier, C., & Reinhardt, D. (2001). Auxin and phyllotaxis. Trends Plant Sci. 6: 187-189.

Landrein, B., Lathe, R., Bringmann, M., Vouillot, C., Ivakov, A., Boudaoud, A., ... & Hamant, O. (2013). Impaired cellulose synthase guidance leads to stem torsion and twists phyllotactic patterns in Arabidopsis. Curr. Biol. 23: 895-900.

Landrein, B., Refahi, Y., Besnard, F., Hervieux, N., Mirabet, V., Boudaoud, A., ... & Hamant, O. (2015). Meristem size contributes to the robustness of phyllotaxis in Arabidopsis. J. Exp. Bot. 66: 1317-1324.

Lee, H., Ganguly, A., Baik, S., & Cho, H. T. (2021). Calcium-dependent protein kinase 29 modulates PIN-FORMED polarity and Arabidopsis development via its own phosphorylation code. Plant Cell 33: 3513-3531.

Lee, J. S., Mulkey, T. J., & Evans, M. L. (1984). Inhibition of polar calcium movement and gravitropism in roots treated with auxin-transport inhibitors. Planta 160: 536-543.

Li, T., Yan, A., Bhatia, N., Altinok, A., Afik, E., Durand-Smet, P., ... & Meyerowitz, E. M. (2019). Calcium signals are necessary to establish auxin transporter polarity in a plant stem cell niche. Nat. Commun. 10: 726.

Lyndon, R. F. (1998). The shoot apical meristem: its growth and development. Cambridge University Press.

Marhava, P., Bassukas, A. E. L., Zourelidou, M., Kolb, M., Moret, B., Fastner, A., ... & Hardtke, C. S. (2018). A molecular rheostat adjusts auxin flux to promote root protophloem differentiation. Nature 558: 297-300.

McCormack, E., Tsai, Y. C., & Braam, J. (2005). Handling calcium signaling: arabidopsis CaMs and CMLs. Trends Plant Sci. 10: 383-389.

Monshausen, G. B., Miller, N. D., Murphy, A. S., & Gilroy, S. (2011). Dynamics of auxin-dependent Ca2+ and pH signaling in root growth revealed by integrating high-resolution imaging with automated computer vision-based analysis. Plant J. 65: 309-318.

Nakayama, N., Smith, R. S., Mandel, T., Robinson, S., Kimura, S., Boudaoud, A., & Kuhlemeier, C. (2012). Mechanical regulation of auxin-mediated growth. Curr. Biol. 22: 1468-1476.

Okada, K., Ueda, J., Komaki, M. K., Bell, C. J., & Shimura, Y. (1991). Requirement of the auxin polar transport system in early stages of Arabidopsis floral bud formation. Plant Cell 3: 677-684.

Peaucelle, A., Morin, H., Traas, J., & Laufs, P. (2007). Plants expressing a miR164-resistant CUC2 gene reveal the importance of post-meristematic maintenance of phyllotaxy in Arabidopsis. Development 6: 1045-50.

Petrásek, J., Mravec, J., Bouchard, R., Blakeslee, J. J., Abas, M., Seifertová, D., ... & Friml, J. (2006). PIN proteins perform a rate-limiting function in cellular auxin efflux. Science 312: 914-918.

Plieth, C., & Trewavas, A. J. (2002). Reorientation of seedlings in the earth's gravitational field induces cytosolic calcium transients. Plant Physiol. 129: 786-796.

Rademacher, E. H., & Offringa, R. (2012). Evolutionary adaptations of plant AGC kinases: from light signaling to cell polarity regulation. Front. Plant Sci. 3: 250.

Reinhardt, D., Mandel, T., & Kuhlemeier, C. (2000). Auxin regulates the initiation and radial position of plant lateral organs. Plant Cell 12: 507-518.

Reinhardt, D., Pesce, E. R., Stieger, P., Mandel, T., Baltensperger, K., Bennett, M., ... & Kuhlemeier, C. (2003). Regulation of phyllotaxis by polar auxin transport. Nature 426: 255-260.

Rigó, G., Ayaydin, F., Tietz, O., Zsigmond, L., Kovács, H., Páy, A., ... & Cséplő, Á. (2013). Inactivation of plasma membrane–localized CDPK-RELATED KINASE5 decelerates PIN2 exocytosis and root gravitropic response in Arabidopsis. Plant Cell 25: 1592-1608.

Roberts, D. M., & Harmon, A. C. (1992). Calcium-modulated proteins: targets of intracellular calcium signals in higher plants. Annu. Rev. Plant Biol. 43: 375-414.

Rudd, J. J., & Franklin-Tong, V. E. (1999). Calcium signaling in plants. Cell. Mol. Life Sci. 55: 214-232.

Santin, F., Bhogale, S., Fantino, E., Grandellis, C., Banerjee, A. K., & Ulloa, R. M. (2017). Solanum tuberosum StCDPK1 is regulated by miR390 at the posttranscriptional level and phosphorylates the auxin efflux carrier StPIN4 in vitro, a potential downstream target in potato development. Physiol. Plant. 159: 244-261.

Sassi, M., & Vernoux, T. (2013). Auxin and self-organization at the shoot apical meristem. J. Exp. Bot. 64: 2579-2592.

Shi, B., Guo, X., Wang, Y., Xiong, Y., Wang, J., Hayashi, K. I., ... & Jiao, Y. (2018). Feedback from lateral organs controls shoot apical meristem growth by modulating auxin transport. Dev. Cell 44: 204-216.

Shih, H. W., DePew, C. L., Miller, N. D., & Monshausen, G. B. (2015). The Cyclic Nucleotide-Gated Channel CNGC14 Regulates Root Gravitropism in Arabidopsis thaliana. Curr. Biol. 25: 3119–3125.

Smith, R. S., Guyomarc'h, S., Mandel, T., Reinhardt, D., Kuhlemeier, C., & Prusinkiewicz, P. (2006). A plausible model of phyllotaxis. Proc. Natl. Acad. Sci. U.S.A. 103: 1301–1306.

Stoma, S., Lucas, M., Chopard, J., Schaedel, M., Traas, J., & Godin, C. (2008). Flux-based transport enhancement as a plausible unifying mechanism for auxin transport in meristem development. PLoS Comput. Biol. 4: e1000207.

Toyota, M., Furuichi, T., Tatsumi, H., & Sokabe, M. (2008). Critical consideration on the relationship between auxin transport and calcium transients in gravity perception of Arabidopsis seedlings. Plant Signal. Behav. 3: 521-524.

Uyttewaal, M., Burian, A., Alim, K., Landrein, B., Borowska-Wykręt, D., Dedieu, A., ... & Hamant, O. (2012). Mechanical stress acts via katanin to amplify differences in growth rate between adjacent cells in Arabidopsis. Cell 149: 439-451.

Vanneste, S., & Friml, J. (2009). Auxin: a trigger for change in plant development. Cell 136: 1005–1016.

Vernoux, T., Brunoud, G., Farcot, E., Morin, V., Van den Daele, H., Legrand, J., ... & Traas, J. (2011). The auxin signalling network translates dynamic input into robust patterning at the shoot apex. Mol. Syst. Biol. 7: 508.

Vernoux, T., Kronenberger, J., Grandjean, O., Laufs, P., & Traas, J. (2000). PIN-FORMED 1 regulates cell fate at the periphery of the shoot apical meristem. Development 127: 5157-5165.

Vogel, H. J. (1994). Calmodulin: a versatile calcium mediator protein. Biochem. Cell Biol. 72: 357-376.

Wisniewska, J., Xu, J., Seifertová, D., Brewer, P. B., Ruzicka, K., Blilou, I., ... & Friml, J. (2006). Polar PIN localization directs auxin flow in plants. Science 312: 883-883.

Xu, T., Niu, J., & Jiang, Z. (2022). Sensing mechanisms: Calcium signaling mediated abiotic stress in plants. Front. Plant Sci.13: 925863.

Xue, Z., Liu, L., & Zhang, C. (2020). Regulation of shoot apical meristem and axillary meristem development in plants. Int. J. Mol. Sci. 21: 2917.

Yin, X. (2021). Phyllotaxis: From classical knowledge to molecular genetics. J. Plant Res. 134: 373-401.

Zhang, J., Vanneste, S., Brewer, P. B., Michniewicz, M., Grones, P., Kleine-Vehn, J., ... & Friml, J. (2011). Inositol trisphosphate-induced Ca2+ signaling modulates auxin transport and PIN polarity. Dev. Cell 20: 855-866.

Zourelidou, M., Absmanner, B., Weller, B., Barbosa, I. C., Willige, B. C., Fastner, A., ... & Schwechheimer, C. (2014). Auxin efflux by PIN-FORMED proteins is activated by two different protein kinases, D6 PROTEIN KINASE and PINOID. Elife 3: e02860.

Zwiewka, M., Bilanovičová, V., Seifu, Y. W., & Nodzyński, T. (2019). The nuts and bolts of PIN auxin efflux carriers. Front. Plant Sci. 10: 985.

Calcium-regulated PINOID kinase activity is required for a robust spiral phyllotaxis in the Arabidopsis inflorescence